PROCEEDINGS OF SPIE

SPIEDigitalLibrary.org/conference-proceedings-of-spie

Evaluation of hyperspectral imaging measurements of changes in hemoglobin oxygenation and oxidation of cytochrome-c-oxidase using a liquid blood phantom

Charly Caredda, Frédéric Lange, Ilias Tachtsidis, Bruno Montcel

Charly Caredda, Frédéric Lange, Ilias Tachtsidis, Bruno Montcel, "Evaluation of hyperspectral imaging measurements of changes in hemoglobin oxygenation and oxidation of cytochrome-c-oxidase using a liquid blood phantom," Proc. SPIE 12628, Diffuse Optical Spectroscopy and Imaging IX, 126280Q (21 August 2023); doi: 10.1117/12.2670746

SPIE.

Event: European Conferences on Biomedical Optics, 2023, Munich, Germany

Evaluation of hyperspectral imaging measurements of changes in hemoglobin oxygenation and oxidation of cytochrome-c-oxidase using a liquid blood phantom

Charly Caredda[a], Frédéric Lange[b], Ilias Tachtsidis[b], and Bruno Montcel[a]

[a]Univ Lyon, INSA-Lyon, Université Claude Bernard Lyon 1, UJM-Saint Etienne, CNRS, Inserm, CREATIS UMR 5220, U1294, F69100, Lyon, France
[b]Department of Medical Physics and Biomedical Engineering, University College London, London, UK

ABSTRACT

Optical imaging is a non-invasive technique that is able to monitor hemodynamic and metabolic responses during neurosurgery. However, a robust quantification is complicated to perform. To overcome this issue, phantoms that mimic biological tissues are required for the development of imaging systems in order to reach a true standardization. In this work, we explore the possibility to use a combined liquid blood phantom with cytochrome contained yeast to evaluate the reliability of hyperspectral imaging to measure oxygenation and metabolic changes. This phantom can be used to verify the reliability of intraoperative optical setups before moving on to clinical application.

Keywords: Hyperspectral imaging; Optical imaging; Blood phantom ; Hemodynamic and metabolic monitoring

1. INTRODUCTION

Optical imaging is a non-invasive technique especially adapted for intraoperative functional brain mapping applications.[1] Hyperspectral cameras combined with a white light illumination allow the analysis of the light attenuation at multiple wavelengths, hence allowing the quantification of the concentration changes in oxy- and deoxygenated hemoglobin (HbO_2 and Hb, respectively) and the oxidative state of the cytochrome-c-oxidase ($oxCCO$) in brain cortex.[2,3]

A robust quantification of these biomarkers is complicated to perform during neurosurgery due the critical context of the operating room, which makes the calibration of optical devices more complex. To overcome this issue, tissue-simulating phantoms are required for the development of medical imaging systems. These phantoms may be used to evaluate, optimize, compare or control imaging systems.[4] Some phantom recipes based on intralipid and blood have emerged to reach that goal.[5] Other phantoms combine a liquid blood phantom with cytochrome-containing yeast to validate measurements of hemodynamic and metabolic activity using NIRS devices.[6] A phantom is important to ensure reliability of measurements across different devices and techniques. Reliable measurements will allow scalability of equipment and ensure robust operation. In this work, we explore the possibility to use a combined liquid blood phantom with cytochrome contained yeast to evaluate the reliability of near infrared hyperspectral imaging to quantify oxygenation and metabolic changes.

The results can be beneficial and useful within the frame-work of our recently started, EU-funded HyperProbe consortium and project,[7,8] which aims at transforming neuronavigation during glioma resection using novel hyperspectral imaging technology.

2. MATERIAL AND METHODS

The experimental setup used in this study is represented in Fig. 1.

Further author information: (Send correspondence to C.C and B.M)
C.C.: E-mail: charly.caredda@creatis.insa-lyon.fr, B.M.: E-mail: bruno.montcel@creatis.insa-lyon.fr

Diffuse Optical Spectroscopy and Imaging IX, edited by Davide Contini, Yoko Hoshi, Thomas D. O'Sullivan, Proc. of SPIE Vol. 12628, 126280Q
 · 0277-786X · doi: 10.1117/12.2670746

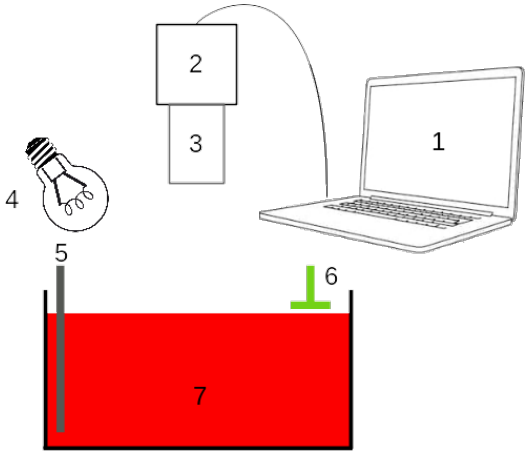

Figure 1. Experimental setup. 1 - Acquisition and processing laptop. 2 - Hyperspectral camera. 3 - Camera Lens. 4 - Halogen bulb. 5 - Oxymeter, temperature and PH probes. 6 - Multi-wavelength time-resolved (TR) domain NIRS system.[6] 7 - Liquid mixture.

2.1 Blood phantom

The blood phantom was developed and validated in previous study[6] by the team at University College London (UCL) Biomedical Optics Research Laboratory (BORL), and mimicks hemodynamic and metabolic changes. The liquid phantom was made of an homogeneous liquid mixture (see Fig. 1 - 7) composed of a solution of 75 mL of Intralipid 20% (IL scattering element), 1425 mL of phosphate buffered saline solution (PBS) and 25 mL of blood (39 $\mu mol.L^{-1}$ of hemoglobin). 10 g of yeast that contained cytochrome was added to the liquid mixture in a second time (see table 1). This recipe provides absorption and diffusion properties similar to those of biological tissue.[5,6] The liquid was poured in a container and homogeneously mixed with a magnetic stirrer. Oxymeter, temperature and pH probes (see Fig. 1 - 5) were used to monitor the liquid mixture during the experiment.

2.2 Data acquisition

Images of the liquid mixture were collected with a hyperspectral camera XIMEA MQ022HG-IM-SM5X5-NIR (integration time: 1 s) combined with an Edmund Optics camera lens (f 1/4 50 mm $f/2$ - $f/22$), see Fig. 1 - 2 and 3. The phantom was illuminated with a continuous wave white light source (OSRAM Classic 116-W 230-V light bulb, see Fig. 1 - 4). This hyperspectral camera collects 25 spectral bands between 675 nm and 975 nm. Data were also collected with a multi-wavelength time-resolved (TR) domain NIRS system (MAESTROS,[6] source-detector distance: 3 cm), see Fig. 1 - 6. 16 wavelengths were collected between 780 nm and 880 nm. To match the spectral range of the TR domain NIRS system, we only kept 8 spectral bands of the hyperspectral camera between 780 nm and 880 nm, see Fig. 2. This spectral range is especially adapted for monitoring ΔC_{Hb}, ΔC_{HbO_2} and ΔC_{oxCCO}.[9,10]

2.3 Experimental paradigm

The experimental paradigm was separated in three cycles (1) (2) and (3). For each cycle, oxy- and deoxygenation events were executed. Data were collected at the end of these events, when hemoglobin was fully saturated (step (a), $SatO_2 = 100\%$) or desaturated with O_2 (step (b), $SatO_2 = 0\%$). During data collection, the magnetic stirrer was stopped. The images were not acquired continuously but sequentially in order to limit the presence of artifacts due to the undulations of the liquid, see Fig. 2. We also used a small region of interest (ROI) of 50×50 pixels to avoid a large dispersion of intensity in hyperspectral images. An example of these images acquired during $SatO_2 = 100\%$ and $SatO_2 = 0\%$ are represented in Fig. 2. The cycles of the experimental paradigm are detailed in table 1. For all cycles, hemoglobin was fully saturated in O_2 during steps (a) by O_2 bubbling. During cycle (1-b), the liquid mixture was yeast free, hemoglobin deoxygenation was induced by N_2 bubbling. For cycles (2-b) and (3-b), yeast has been added to the liquid mixture, hemoglobin deoxygenation was provoked by the consumption of O_2 by the yeast.

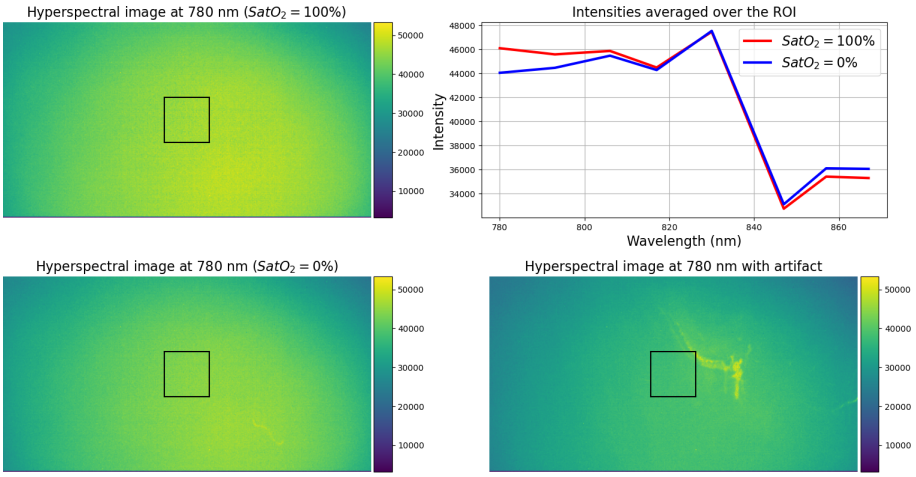

Figure 2. Hyperspectral image at 780 nm of the blood phantom with and without artifact. The ROI used in hyperspectral images is represented with a black square. On the top right graph, we represented the intensities averaged over the ROI for $SatO_2 = 100\%$ and $SatO_2 = 0\%$.

Cycle ID	Addition to the liquid mixture described in section 2.1	Blood phantom $SatO_2$ (%)	
		Step (a)	Step (b)
1		100% (O_2 bubbling)	0% (N_2 bubbling)
2	10 g of yeast	100% (O_2 bubbling)	0% (O_2 consumption by the yeast)
3	25 mL of blood	100% (O_2 bubbling)	0% (O_2 consumption by the yeast)

Table 1. Experimental paradigm conducted during the phantom experiment.

2.4 Quantification of chromophores

Concentration changes of Hb, HbO_2, HbT and $oxCCO$ were calculated with the modified Beer-Lambert law. For each cycle, the baseline for the calculation of the absorbance changes corresponded to data averaged during the step (a). We considered the spectral sensitivities of the light source and the camera channels in the Beer-Lambert model.[1,3] The pathlength used in the quantification algorithm was calculated with TR domain NIRS system during cycle (1-a) with a source-detector distance of 3 cm (the same pathlength was used for all measurements).

For each chromophore, matrices of concentration changes of size $50 \times 50 \times T_a$ and $50 \times 50 \times T_b$ were obtained during steps (a) and (b), respectively. 50×50 is the size of the ROI (see Fig. 2) and T_a or T_b the temporal definition of steps (a) or (b), respectively. Temporal mean and standard deviation of the concentration changes were calculated over the ROI, which leads to vectors $m(\Delta C_n)_{T_i}$ and $\sigma(\Delta C_n)_{T_i}$, respectively. These vectors have size T_i which is equal to T_a or T_b.

2.5 Statistical analysis

To evaluate the difference in means between concentration changes measured in steps (a) versus steps (b), T-tests were computed to compare the sample $m(\Delta C_n)_{T_a}$ to $m(\Delta C_n)_{T_b}$ at 1% significance level.

During steps (b), hemoglobin was fully desaturated. So we expect to observe a decrease of $m(\Delta C_{HbO_2})_{T_b}$ compared to $m(\Delta C_{HbO_2})_{T_a}$ and an increase of $m(\Delta C_{Hb})_{T_b}$ compared to $m(\Delta C_{Hb})_{T_a}$. We expect to see no differences in means between $m(\Delta C_{HbT})_{T_a}$ and $m(\Delta C_{HbT})_{T_b}$ since hemoglobin was fully desaturated during steps (b). Since the blood phantom was yeast free during cycle (1), we expect to see no differences between $m(\Delta C_{oxCCO})_{T_a}$ and $m(\Delta C_{oxCCO})_{T_b}$ during cycle (1). Yeast was added at cycle (2), so we expect to observe a decrease of $m(\Delta C_{oxCCO})_{T_b}$ compared to $m(\Delta C_{oxCCO})_{T_a}$ during cycles (2) and (3). This leads to the following hypotheses ($\overline{m(\Delta C_n)_{T_i}}$ represents the average value of $m(\Delta C_n)_{T_i}$):

$$
HbO_2 : \begin{cases} H_0 & \overline{m(\Delta C_{HbO_2})_{T_a}} = \overline{m(\Delta C_{HbO_2})_{T_b}} \\ H_1 & \overline{m(\Delta C_{HbO_2})_{T_a}} > \overline{m(\Delta C_{HbO_2})_{T_b}} \end{cases} \qquad Hb : \begin{cases} H_0 & \overline{m(\Delta C_{Hb})_{T_a}} = \overline{m(\Delta C_{Hb})_{T_b}} \\ H_1 & \overline{m(\Delta C_{Hb})_{T_a}} < \overline{m(\Delta C_{Hb})_{T_b}} \end{cases}
$$
$$
HbT : \begin{cases} H_0 & \overline{m(\Delta C_{HbT})_{T_a}} = \overline{m(\Delta C_{HbT})_{T_b}} \\ H_1 & \overline{m(\Delta C_{HbT})_{T_a}} \neq \overline{m(\Delta C_{HbT})_{T_b}} \end{cases} \qquad oxCCO : \begin{cases} H_0 & \overline{m(\Delta C_{oxCCO})_{T_a}} = \overline{m(\Delta C_{oxCCO})_{T_b}} \\ H_1 & \overline{m(\Delta C_{oxCCO})_{T_a}} > \overline{m(\Delta C_{oxCCO})_{T_b}} \end{cases} \tag{1}
$$

3. RESULTS

In Fig. 3, temporal concentration changes are represented for each cycle. During deoxygenation steps (steps (b) in blue), $m(\Delta C_{HbO_2})$ and $m(\Delta C_{Hb})$ values decreased and increased respectively. For $m(\Delta C_{HbO_2})$, values are roughly the same during steps (1-b) and (2-b) but are approximately two times smaller during step (3-b). For $m(\Delta C_{Hb})$, values increased linearly. For $m(\Delta C_{HbT})$, values oscillate between $0\mu mol.L^{-1}$ during cycle (1), and increased during steps (2-b) and (2-c). For $m(\Delta C_{oxCCO})$, values oscillate between $0\mu mol.L^{-1}$ during cycle (1), and decreased during steps (2-b) and (2-c).

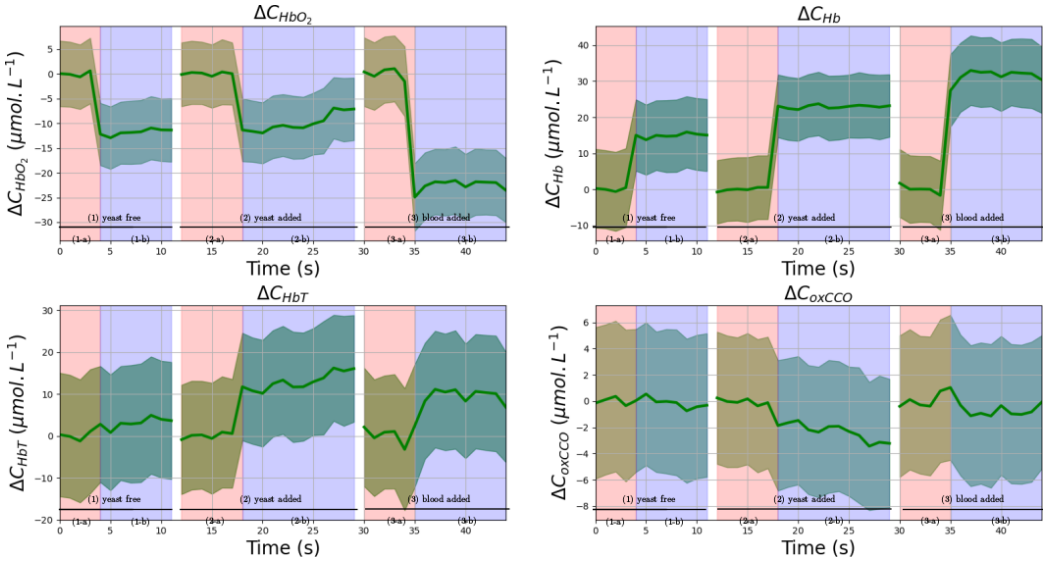

Figure 3. Temporal concentration changes computed with hyperspectral imaging. Mean values ($m(\Delta C_n)$) are represented by solid lines and the dispersion range ($\sigma(DeltaC_n)$) by green shaded areas. Steps (a) are indicated in red ($SatO_2 = 100\%$), these steps are used as baseline in the modified Beer-Lambert law. Steps (b) are indicated in blue ($SatO_2 = 0\%$).

P-values computed when testing the difference in means between concentration changes measured in steps (a) versus steps (b) are indicated in table 2. For HbO_2, Hb and HbT, p-values were less than 1% for all cycles, the null hypothesis was rejected. For $oxCCO$, the p-value calculated for cycles (1) and (3) was greater than 1%, the null hypothesis could not be rejected. For cycle (2), the p-value was less than 1%, the null hypothesis was rejected.

Chromophore	Cycle (1)	Cycle (2)	Cycle (3)
HbO_2	$7e-12^*$	$2e-10^*$	$3e-15^*$
Hb	$5e-13^*$	$4e-24*$	$6e-15^*$
HbT	$5e-4^*$	$3e-11^*$	$1e-5^*$
$oxCCO$	0.28	$1e-7^*$	0.07

Table 2. P-values obtained with T-tests and hypotheses detailed in Eq. (1). Values labeled with * indicated that the null hypothesis was rejected at 1% significance level. P-values written in red indicates that the statistical comparison is consistent with expectations described in section 2.5.

4. DISCUSSION AND CONCLUSION

In Fig. 3 and table 2, we show that a blood phantom based on commercial yeast can be used to validate measurements performed with a hyperspectral camera. The camera is able to monitor concentration changes in HbO_2 and Hb, but measurements are subject to large errors. Indeed, we should not observe variations in ΔC_{HbT} during steps (b), but this hypothesis could not be rejected, see table 2. The measurements were very noisy which makes the quantification of ΔC_{oxCCO} complex. During cycle (1), the liquid mixture was yeast free, and measurements showed no differences between steps (a) and (b). For cycle (2), yeast was added to the mixture. During step (b) (desaturation), ΔC_{oxCCO} response significantly dropped. These results corresponded to the expected physiological response. However, for cycle (3-b), we did not observe a significant decrease of ΔC_{oxCCO}. In order to understand the discrepancies between the measurements given by the hyperspectral camera and what is physiologically expected, we must relate its results to the data acquired by the TR domain NIRS system MAESTROS.

To conclude, we show that a blood phantom and commercial yeast can be used to validate the measurement of ΔC_{HbO_2}, ΔC_{Hb} and ΔC_{oxCCO} using near infrared hyperspectral imaging. This homogeneous phantom provides an excellent means of verifying the reliability of intraoperative optical setups before moving on to clinical application.

5. ACKNOWLEDGEMENTS

These works were funded by the European Union's Horizon Europe research and innovation programme under grant agreement No 101071040 – project HyperProbe; LABEX PRIMES (ANR-11-LABX-0063) of Université de Lyon, within the program "Investissements d'Avenir" (ANR-11-IDEX-0007), operated by the French National Research Agency (ANR); Infrastructures d'Avenir en Biologie Santé (ANR-11-INBS-000), within the program "Investissements d'Avenir" operated by the French National Research Agency (ANR) and France Life Imaging (ANR-11-INBS-0006). FL and IT are supported by UCL, which, as UK participant in Horizon Europe Project HyperProbe is supported by UKRI grant number 10048387.

REFERENCES

[1] Caredda, C. et al., "Intraoperative quantitative functional brain mapping using an rgb camera," *Neurophotonics* **6**(4), 045015 (2019).

[2] Giannoni, L. et al., "A hyperspectral imaging system for mapping haemoglobin and cytochrome-c-oxidase concentration changes in the exposed cerebral cortex," *IEEE Journal of Selected Topics in Quantum Electronics* **27**(4), 1–11 (2021).

[3] Caredda, C. et al., "Intraoperative functional and metabolic brain mapping using hyperspectral imaging," in [*Clinical and Translational Neurophotonics 2020*], Madsen, S. J., Yang, V. X. D., and Thakor, N. V., eds., **11225**, 112250B, International Society for Optics and Photonics, SPIE (2020).

[4] Pogue, B. W. et al., "Review of tissue simulating phantoms for optical spectroscopy, imaging and dosimetry," *Journal of biomedical optics* **11**(4), 041102 (2006).

[5] Kleiser, S. et al., "Comparison of tissue oximeters on a liquid phantom with adjustable optical properties," *Biomedical optics express* **7**(8), 2973–2992 (2016).

[6] Lange, F. et al., "Maestros: a multiwavelength time-domain nirs system to monitor changes in oxygenation and oxidation state of cytochrome-c-oxidase," *IEEE Journal of Selected Topics in Quantum Electronics* **25**(1), 1–12 (2018).

[7] "Hyperprobe project." https://hyperprobe.eu/. Accessed: 2023-01-11.

[8] "Hyperprobe project." https://cordis.europa.eu/project/id/101071040. Accessed: 2023-01-11.

[9] Bale, G. et al., "From jöbsis to the present day: a review of clinical near-infrared spectroscopy measurements of cerebral cytochrome-c-oxidase," *Journal of biomedical optics* **21**(9), 091307 (2016).

[10] Caredda, C. et al., "Optimal spectral combination of a hyperspectral camera for intraoperative hemodynamic and metabolic brain mapping," *Applied Sciences* **10**(15) (2020).